PCCP

PAPER

View Article Online
View Journal | View Issue

Cite this: *Phys. Chem. Chem. Phys.*, 2015, **17**, 25133

The composition effect on the optical properties of aqueous synthesized Cu–In–S and Zn–Cu–In–S quantum dot nanocrystals†

Butian Zhang,‡[a] Yucheng Wang,‡[a] Chengbin Yang,[a] Siyi Hu,[b] Yuan Gao,[a] Yiping Zhang,[a] Yue Wang,[b] Hilmi Volkan Demir,[a] Liwei Liu[b] and Ken-Tye Yong§*[a]

Multiternary quantum dots (QDs), because of the large degree of freedom in their structure and composition, have a wide tunability in their bandgap but also exhibit an increased uncertainty and complexity in their optical properties. In this work, we synthesized the ternary Cu–In–S (CIS) and quaternary Zn–Cu–In–S (ZCIS) QDs with different composition ratios *via* a facile aqueous route. The CIS QDs show multi-peak photoluminescence with their peak intensity dependent on the Cu : In ratio, which was illustrated using a donor–acceptor pair recombination process. Upon incorporation of Zn into the CIS QDs under similar conditions, the acquired ZCIS QDs exhibit blue-shifted photoluminescence (PL) spectra with an enhanced emission intensity and a narrowed spectral width (~100 nm). A comparative study reveals that, reducing the Cu : In ratio in the CIS QDs and increasing the Zn content in the alloyed ZCIS QDs are both feasible strategies for bandgap engineering, although the influences on optical properties of the QDs were different. The XRD and EDX spectra revealed that the widening of the bandgap of the ZCIS QDs was correlated with the alloyed nanostructures and the preferential substitution of Cu by Zn. Compared to the Cu : In ratio variation, incorporation of Zn into CIS QDs is an effective strategy to achieve a more homogeneous absorption band and a wide range of emission wavelength tunability. After ZnS shell coating, the ZCIS/ZnS QDs show a further enhanced PL intensity with a prolonged fluorescence lifetime. Unlike CIS QDs, the blue shift in PL upon the shell growth was not pronounced for ZCIS QDs, for which a surface reconstruction mechanism was proposed and discussed. Finally, the as-prepared ZCIS/ZnS QDs were employed for *in vitro* cell imaging and exhibited good biocompatibility to macrophage cells.

Received 8th June 2015,
Accepted 2nd September 2015

DOI: 10.1039/c5cp03312h

www.rsc.org/pccp

1. Introduction

Colloidal quantum dots (QDs) have found widespread biomedical applications since 1998 owing to the rapid development of colloidal synthesis and functionalization methods.[1–6] However, most of the high-quality QDs developed so far have been composed of heavy metal elements including Cd, Pb, As, and Hg. These heavy metal elements raise tremendous concerns to the biomedical community about the toxicity of these QDs,[7,8] especially if the heavy metal ions are released from the degraded QDs during *in vivo* or clinical applications.[9] Development of QDs composed of less toxic compositions, such as InP, $CuInS_2$, Ag_2S, Si and C-based QDs, is a potential strategy to deal with the heavy metal-related toxic effects.[10–14] Unfortunately, the preparation of Cd-free QDs having comparable optical properties with the conventional QDs remains a challenge to date. For example, the size-tunable emission covering the whole visible range is typically no longer a characteristic property of some Cd-free QDs.[15,16] For this reason, other strategies are required to be developed to adjust the bandgap or tune the emission wavelength of the Cd-free nanocrystals. Additionally, in comparison to the low-cost and greener aqueous method for the preparation of Cd QDs,[17] most of the synthesis procedures of Cd-free QDs are much trivial, due to the need for high reaction temperature, volatile and hazardous ligands or pyrophoric precursors.[18,19]

To make the bandgap and emission wavelength of the QDs more adjustable, multi-ternary semiconductor materials have been studied due to their large degree of freedom in the composition and lattice structure.[20] For example, by substituting the Zn(II) atoms

[a] *School of Electrical and Electronic Engineering, Nanyang Technological University, Singapore 639798, Singapore*
[b] *Changchun University of Science and Technology, Changchun, Jilin 130022, P. R. China*

† Electronic supplementary information (ESI) available: Additional tables and figures. See DOI: 10.1039/c5cp03312h

‡ These authors contributed equally.

§ School of Electrical and Electronic Engineering, Nanyang Technological University, Singapore 639798, Singapore. E-mail: ktyong@ntu.edu.sg; Tel: +65-6790-5444.

in ZnS with Cu(I) and In(III) atoms, the ternary Cu–In–S (CIS) preserves the semiconductor properties but narrows the bandgap from 3.68 to 1.55 eV.[21] For Zn–Cu–In–S (ZCIS) preparation, the substitution of the Cu and In atoms partly by Zn atoms could result in bandgap energy that lies between CIS and ZnS (2.34 eV for $CuInZn_2S_4$[20]).[22] Owing to their large tolerance of element off-stoichiometry, the bandgap of CIS and ZCIS could be further adjusted by tuning the composition ratio.[23,24] Based on these bandgap adjustment strategies, researchers have already developed CIS and ZCIS QDs with emissions tunable from the visible to near-infrared region.[23,25] However, as the structural and composition freedom increases, more configurations and impurity phases tend to coexist in the multi-ternary materials. Based on the calculation results, a small deviation of the element stoichiometry will generate secondary phases (*e.g.*, CuS, Cu_2S, ZnS) and other impurity phases (*e.g.*, vacancies, interstitials, antisites) in quaternary materials.[26,27] Correspondingly, multi-peak or broad PL profiles for the CIS and ZCIS QDs have been observed in many reported experimental studies,[28,29] which suggest the coexistence of the multi-phases or the inhomogeneity of composition. Moreover, the poor comparability of the optical properties and crystal structures of CIS or ZCIS QDs reported in different studies also implies the complexity and uncertainty of the making of multi-ternary nanocrystals. Therefore, when developing different synthesis methods for preparing these multi-ternary nanocrystals, a systematic investigation is needed to understand the effect of the composition ratio on their optical and structural properties.

A hot colloidal synthesis method has been successfully developed to prepare CIS and ZCIS QDs in the organic phase at temperatures of 200–250 °C.[23,30] On the contrary, only handful studies reported preparing CIS QDs in an aqueous solvent at a relatively low temperature of around 95–150 °C.[31–33] The aqueous synthesis method usually requires inexpensive precursors and a simpler synthesis setup. More importantly, using water as a reaction medium minimizes the toxicity issue associated with organic solvent evaporation. Furthermore, the as-synthesized QDs are water-dispersible and can be directly used for biological applications after careful washing. Comparatively, the CIS and ZCIS QDs prepared in the organic phase need to be transferred into the aqueous phase. Since these CIS and ZCIS QDs are capped with oleic acid and organothiols, it is difficult to make them water dispersible by ligand exchange. On the other hand, phase transfer *via* an encapsulation method usually results in nanoparticle agglomeration or a significant size increase.[34–36] Nowadays, the aqueous synthesis method for Cd-based QDs has been well developed, and optical properties of the QDs are comparable with the ones synthesized in an organic solvent.[37–39] On the contrary, synthesis of aqueous CIS QDs is still in their infancy stage. Some of the QDs exhibit no PL or low PL efficiency with untunable emission wavelength,[31] while improvements have been made and reported in recent studies.[32,33] Zn alloying is expected to strengthen the crystal structures and eliminate the defects of the CIS QDs. Although controlling of the bandgap and optical properties by varying Zn concentration has been demonstrated in the organic method,[40,41] as far as we know, only one manuscript has reported the aqueous synthesis of ZCIS QDs. In the work, bright Cu doped In–Zn–S QDs were prepared using an autoclave at 150 °C for 23 h.[42] To our best knowledge, no work has been reported on ZCIS QD preparation *via* a low-temperature water bath route. Compared to a hot colloidal synthesis method requiring high temperature treatment in the presence of argon/nitrogen or an autoclave method requiring high temperature and pressure treatment, the set-up of the water bath route is simpler, and the process is greener.

In this work, we employed a quick and facile aqueous phase synthesis method to prepare the ternary CIS and quaternary ZCIS QDs. The CIS QDs show multi-peak photoluminescence with their peak intensity dependent on the Cu : In ratio. Compared to these CIS QDs, the ZCIS QDs synthesized under similar conditions exhibit enhanced PL and narrower spectral widths within a certain range of Zn content. The evolution of absorption and emission spectra of the ZCIS QDs when changing the Zn contents was analyzed and correlated with their structural and compositional properties. Based on our results, the influence of the Cu : In ratio and Zn content on the optical properties of the QDs was compared and discussed. Next, the deposition of ZnS shells on ZCIS QDs resulted in further enhanced PL intensity together with a lengthened fluorescence lifetime of the QDs. Finally, the resulted ZCIS/ZnS QDs were applied for cell imaging and these nanocrystals showed low toxicity to macrophage cells.

2. Experimental

2.1 Materials

Copper(II) chloride ($CuCl_2$, 99%), indium(III) chloride tetrahydrate ($InCl_3 \cdot 4H_2O$, 97%), zinc acetate ($Zn(OAc)_2$, 99.99%), 3-mercaptopropionic acid (MPA, ≥99%) and ammonium hydroxide solution (NH_4OH, 28.0–30.0%) were purchased from Sigma-Aldrich. Sodium sulfide hydrate ($Na_2S \cdot xH_2O$, 60–62%) was obtained from ACROS Organics. All chemicals were used as received. Deionized water (DI water, 18.2 MΩ cm) was used throughout the experiment.

2.2 Synthesis of CIS/ZnS QDs

In a typical procedure for synthesizing Cu–In–S(CIS) QDs with a Cu : In ratio of 0.6, aqueous solution of $InCl_3$ (0.025 mmol) was mixed with MPA (0.2 mmol) in 20 mL of DI water and the pH was adjusted to 9 using NaOH. Afterwards, 0.5 mL of ammonium hydroxide solution of $CuCl_2$ (0.015 mmol) with MPA (0.3 mmol) were added to the solutions. Subsequently the Na_2S solution (0.04 mmol) was injected into the mixtures at room temperature. The reaction mixtures were heated to 100 °C and kept at this temperature for 45 min. Then, 0.25 mL of 0.04 M $Zn(OAc)_2$ and 0.25 mL of 0.04 M Na_2S solutions were slowly injected into the reaction mixtures four times to obtain CIS/ZnS QDs. The QDs were washed with ethanol at a volume ratio of 1 : 2 before use. To synthesize the CIS/ZnS QDs with different Cu : In ratios, the feed ratio of Cu : In was adjusted from 0.07 to 1.33 while the amount of MPA was set at the moles of 20Cu + 8In.

2.3 Synthesis of ZCIS/ZnS QDs

In a typical synthetic reaction of Zn–Cu–In–S(ZCIS) QDs with a Zn content of 30% and a Cu : In ratio of 0.6, $Zn(OAc)_2$ (0.012 mmol) and $InCl_3$ (0.0175 mmol) were mixed with MPA (0.164 mmol) in 20 mL of DI water. The pH value of the mixture was adjusted to the range of 9–10 by adding NaOH. Then, 0.03 M ammonia solution of $CuCl_2$ (0.0105 mmol) with MPA (0.21 mmol) were injected into the mixtures. Afterwards, Na_2S solution (0.04 mmol) was added in the solutions and the reaction solution was heated to 100 °C. Following the growth of the QDs at 100 °C for 40 min, the ZnS shell was coated on the ZCIS QDs. Before use, the QDs were washed with ethanol. The ZCIS/ZnS QDs with different Zn content could be obtained by varying the feed ratio of Zn : (Cu + In) while keeping the gross amount of the metal precursors at 0.04 mmol. The amount of MPA was set at the moles of 20Cu + 8In + 2Zn.

2.4 Characterization

Transmission electron microscopy (TEM) images were obtained using a FEI Tecnai™ microscope operating at 200 kV. The absorption and photoluminescence (PL) spectra of the synthesized QDs were collected using a UV-2450 spectrometer (Shimadzu) and a Fluorolog-3 Fluorometer (HORIBA Jobin Yvon, Edison). To determine the quantum yield (QY) of the samples, CdSe QDs in chloroform were firstly measured as a reference sample. QY of CdSe QDs was calculated by comparing the integrated emission with that of the Rhodamine 6G in ethanol under 480 nm excitation. The QY of the synthesized QDs was then determined by comparing with the CdSe QDs at the same excitation wavelengths. Energy dispersive X-ray spectroscopy (EDX) was performed using a JSM-5600LV scanning electron microscope equipped with an EDX detector. Samples are carefully washed before measurement. The powder XRD patterns of the QDs were recorded on a Siemens D5005 X-ray diffractometer. The luminescence decay curve was obtained using a DCS-120 confocal scanning fluorescence lifetime imaging system (excitation wavelength: 375 nm, repetition rates: 20 MHz). Hydrodynamic diameter of the QDs was measured using a 90Plus particle size analyzer (Brookhaven Instruments) using the DLS technique.

2.5 Cell imaging and cell viability studies

RAW264.7 macrophages were cultured in DMEM supplemented with 10% fetal bovine serum (FBS, Hyclone), penicillin (100 μg mL^{-1}, Gibco) and streptomycin (100 μg mL^{-1}, Gibco) at 37 °C with 5% CO_2. For the cell imaging study, the cells seeded on to a 6-well plate were incubated with 30% ZCIS/ZnS QDs for 4 h. Afterwards, the treated cells were washed with PBS buffer three times and fixed using the 4% formaldehyde solution. The nuclei of the cells were stained with 4′,6-diamidino-2-phenylindole dihydrochloride (DAPI, Sigma). The cell viability of RAW264.7 macrophages treated with QDs was performed using MTT (3-(4,5-dimethylthiazol-2-yl)-2,5-diphenyltetrazolium bromide, Life Technologies) assay. Cells seeded in 96-well plates were incubated with 30% ZCIS/ZnS solutions with different concentrations for 24 h. Afterwards, 20 μL of MTT solution (5 mg mL^{-1}) was added to each well. After another 4 h of incubation, the solution in the wells was removed and the purple precipitate was dispersed in 150 μL of dimethyl sulfoxide (DMSO, Sigma). The absorbance of the solution in the wells was measured using a Bio-Rad microplate reader at a wavelength of 490 nm. The cell viability was calculated by normalizing the absorbance of the sample wells to that of the control wells.

3. Results and discussion

3.1 Effect of the Cu : In ratio on the optical properties of Cu–In–S (CIS) QDs

CIS QDs with less structural complexity were firstly synthesized to provide guidance for the study of ZCIS QDs. Because ternary CIS structures could accommodate large off-stoichiometry[23] by forming the antisites (In_{Cu}, Cu_{In}), interstitial sites (Cu_i, In_i) or vacancies (V_{Cu}, V_{In}, V_S), the diversity of the CIS lattice structures facilitates continuous tuning of the optoelectronic properties, which, on the other hand, also raise difficulty in generating CIS products with a pure phase. In comparison with their bulk counterpart, this challenge is more pronounced for CIS QD materials, because the QDs are so small that even fewer defects or impurity phases could introduce a great difference in their properties.[43] For this reason, varied optical properties and crystal structures have been reported when the synthesis conditions were slightly changed. In this work, a facile synthesis method was optimized in aqueous solution at a growth temperature of 100 °C. The Cu : In feed ratio was studied in a range of 0.07–1.3, and the amount of the stabilizing ligands (MPA) was optimized to achieve high PL efficiency and colloidal stability. EDX measurements determined the Cu : In ratio in the final QD products, which shows an increasing trend when elevating the Cu : In feed ratio (Fig. 1e). High-resolution TEM images (Fig. S1, ESI†) and TEM images (Fig. 1a) reveal that the as-prepared CIS QDs are highly crystalline. And the sizes are estimated to be 4.5 ± 0.7 nm (Fig. 1a, upper inset). The interplanar spacings measured from their FFT pattern are 0.32 nm and 0.20 nm, consistent with the (112) and (204) faces of the tetragonal CIS phase (JCPDS 27-0159) determined by the XRD pattern (given and discussed later in Fig. 3). As can be observed in Fig. 1b, absorption spectra of the QDs shifted to shorter wavelengths in the range of 400–700 nm as the Cu : In ratio decreases, indicating widening of the bandgap under a Cu-poor condition.[29,44] On the other hand, the absence of distinct exciton features in absorption spectra can be attributed to a joint effect of broad size distribution, irregular composition distribution and the existence of various intra-band-gap states.[45] As shown in photoluminescence spectra (Fig. 1c), the prepared QDs exhibit a broad emission centered at ~700 nm accompanied by a narrow emission at 532 nm. As the Cu : In feed ratio increases from 0.07 to 1.33, the emission at 700 nm was firstly enhanced and then reached a maximum value at Cu : In = 0.6, while further increasing the Cu component will lead to a PL QY decrease (Fig. 1g). On the other hand, elevating the Cu : In feed ratio caused a decrease of the 532 nm emission intensity (Fig. 1f). Previous reports on CIS QDs

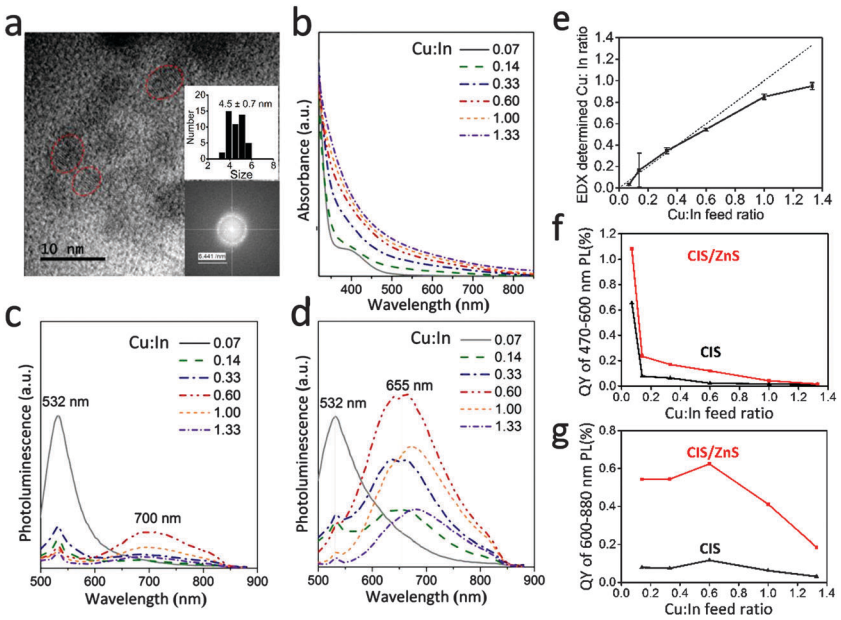

Fig. 1 Characterization of CIS QDs. (a) Representative TEM image, size distribution (upper inset) and the FFT pattern (lower inset) of CIS QDs with a Cu : In ratio of 0.6. (b) Absorption and (c) photoluminescence spectra (450 nm excitation) of CIS QDs with respect to the Cu : In feed ratio of 0.07–1.33, as given in the legend. (d) Photoluminescence spectra of the same CIS/ZnS QDs. (e) EDX determined Cu : In ratio in the synthesized CIS QDs as a function of their corresponding feed ratio (dash line). (f) and (g) QY of the CIS and CIS/ZnS QDs within the range of 470–600 nm and 600–880 nm.

synthesis have shown wide variations in their PL properties. Some research groups have obtained deep red-emitting CIS QDs (650–700 nm)[29,31,45] while the others observed that the emissions can be extended to the near-infrared range of 700–800 nm.[28,44] Moreover, in a recent work, aqueous CIS QDs have also been prepared with yellow-green emission peaks at 530 nm.[32] Typically, the red-NIR emission was attributed to the donor–acceptor pair (DAP) transition, where In_{Cu}/V_S and V_{Cu} served as a donor and an acceptor, respectively. Considering the energy level of the defect states, the deep red emission was most probably caused by the transition from the conduction band or V_S to V_{Cu}, while the NIR emission may originate from the In_{Cu}–V_{Cu} transition.[29,45] According to Chen *et al.*, optimized PL emission of CIS QDs was achieved at Cu : In = 0.7, which was thought to be an optimal ratio for accommodating maximum In_{Cu}–V_{Cu} pairs.[23] A similar result was obtained in our work, as the maximum intensity of 700 nm emission was obtained at a Cu : In feed ratio of 0.6. Based on the above discussion, the 700 nm emission here should be mainly attributed to the DAP transition of the In_{Cu}–V_{Cu} pairs. The mechanism for the green emission at 532 nm is not clear. Because the green emission becomes prominent under a Cu-poor and In-rich condition, it may originate from the band-edge transition or defect related emission of In_xS_y species. A similar property has been observed in In_2S_3 nanospheres or thin films.[46–48]

After deposition of an additional ZnS shell layer coating over the CIS cores, the QY of the red emission of the obtained CIS/ZnS QDs was 6–8 fold enhanced and the peak wavelength was blue-shifted by 8–45 nm (Fig. 1g). The significant PL enhancement can be attributed to passivation of the surface defects by the ZnS shell. As for the pronounced blue shift, several mechanisms were proposed including the interdiffusion of Zn and surface reconstruction. Interdiffusion of Zn often proceeds *via* cation exchange, in the presence of free Zn precursors and at a high temperature.[34,49] Considering the relatively low temperature (100 °C) applied in our method, the interdiffusion was unlikely to take place.[11,50] Surface reconstruction involves partially cation exchange and crystal deformations at the core–shell interface. Although Zn is not expected to diffuse into the core, it may replace Cu and In on the core surface. Since a large proportion (~30%) of atoms are located on the surface for a CIS QD of 5 nm diameter,[51] this partial cation exchange process may have an impact on the emission wavelength. Crystal deformation is suggested as another possible cause for the PL blue shift. Because of the difference in lattice parameters between CIS (a = 5.523 Å) and ZnS (a = 5.406 Å), compressive strain can appear on the CIS core after shell coating, which will lead to a widening of the bandgap.[52,53] In a recent report, Kraatz *et al.* investigated the PL mechanism of hydrophobic CIS/ZnS QDs and attributed the PL donor as In_{Cu} rather than the V_S or conduction band.[54] The V_S to V_{Cu} transition was considered to make a contribution to the PL of CIS core QDs while this recombination pathway should be suppressed in CIS/ZnS QDs.

3.2 Effect of the Zn content on the optical properties of Zn–Cu–In–S (ZCIS) QDs

As for the proposed ZCIS QD preparation, different amounts of the Zn precursor were added in reaction solutions while the Cu : In feed ratio was fixed at 0.6. From the TEM image (Fig. 2a and lower inset), the synthesized ZCIS QDs are crystalline and monodisperse nanocrystals with an average size of 4.9 ± 0.6 nm (Fig. 2a, upper inset). The absorption and emission spectra of the synthesized ZCIS QDs were analysed and correlated with

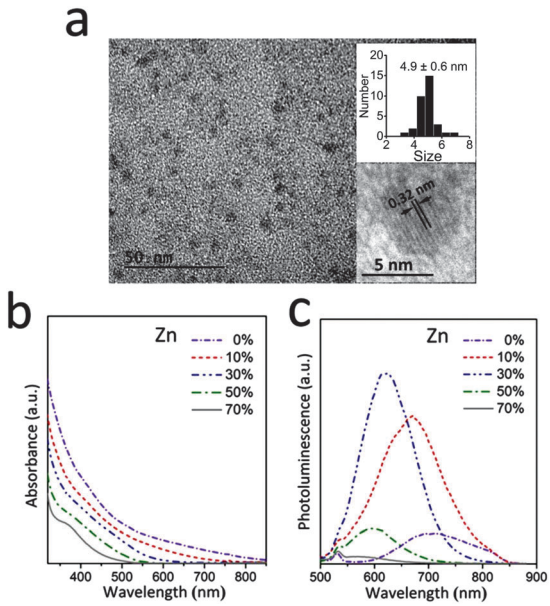

Fig. 2 (a) TEM image, size distribution (upper inset) and the HRTEM image (lower inset) of 30% ZCIS QDs. (b) Absorption and (c) photoluminescence spectra of ZCIS QDs with 0–70% Zn content.

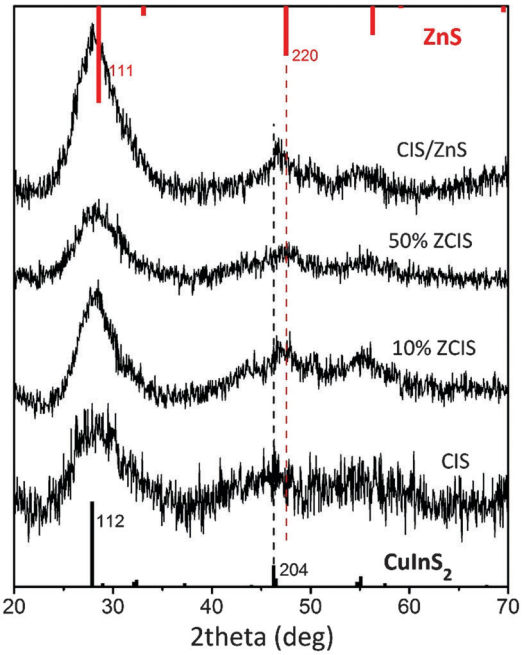

Fig. 3 X-ray diffraction patterns of CIS QDs, 10% ZCIS QDs, 50% ZCIS QDs and CIS/ZnS QDs.

compositional and structural characterization. As shown in Fig. 2b, absorption spectra of the ZCIS QDs gradually shifted to shorter wavelengths with increasing Zn content. The blue-shift of the absorbance profile indicates widening of the bandgap as a result of the Zn incorporation.[29] In a recent report by Pan *et al.*, the bandgap of ZCIS nanocrystals with varying Zn content has been described and predicted as a function of the bandgaps of the CIS and ZnS compounds.[21] In this work, an alloyed structure of our QDs was investigated using XRD spectroscopy. Fig. 3 shows the XRD spectra of the synthesized CIS and ZCIS QDs. The XRD peaks of the CIS QD samples are compatible with the typical diffraction peaks of the tetragonal $CuInS_2$ pattern (JCPDS 27-0159). When Zn was introduced at a content ratio of 10%, the diffraction peaks of the nanocrystals shifted to larger angles and lied between those patterns of $CuInS_2$ and ZnS (JCPDS 05-0566). A more significant right-shift can be observed when the Zn content increased to 50%. On the contrary, shift of the spectra was not that apparent in CIS/ZnS QDs, although the Zn feed content was the same as that of the ZCIS QDs (Zn = 50%). The continuous shift of XRD spectra in ZCIS QDs was attributed to the incorporation of Zn into the CIS crystal lattice.[22,55,56] As suggested by EDX measurements, the Cu : In ratio reduced as a result of the Zn incorporation, which may also have contributed to the blue-shift of the absorbance spectra. According to the EDX results (representatively shown in Fig. 4a) summarized in Table S1 (ESI†), the proportion of Zn in the QDs is approximated to the Zn precursor feeding ratio (Fig. 4b, red line), while the Cu : In ratio showed a decreasing trend as the Zn content increased (Fig. 4b, black line). This phenomenon reveals that, when forming a ZCIS alloyed structure, the Cu sites are more preferable than the In sites to be occupied by Zn atoms. The asymmetric substitution is a result of the energetically favorable formation of Zn_{Cu} substitutes and the weaker strength of the Cu–S bond as compared to the In–S bond.[29,57,58]

As for PL emission spectra, a significant enhancement of PL intensity was observed when the QD was incorporated with 10% and 30% of Zn, while further increasing the Zn content led to a PL decrease (Fig. 2c). Similarly, dependence of the PL intensity on the Zn composition ratio has also been reported for ZCIS QDs forming in the organic phase. For example, in a work reported by Nakamura *et al.*, the PL emission of ZCIS QDs reached a maximum value when the Zn content was around 20–33% (Cu : Zn = 1–2).[57] A possible explanation for this phenomenon is that the incorporation of Zn reduced the structural defects, stabilized the crystal structure and inhibited the nonradiative recombination.[41,56] However, when a high level Zn substitution was taking place, the impurity phases, which induce radiative recombination, may also be eliminated. As a result, further increasing the Zn content resulted in a lower PL intensity from the QDs. In addition to the changes in PL intensity, the full-width-at-half-maximum (FWHM) of the emission spectra decreased from 158 to 105 nm as the Zn content increased from 0% to 50% (Fig. 5, red line), which means that a more homogeneous irradiation was achieved upon incorporating Zn into the crystal nanostructure. Meanwhile, we observed that the PL peak shifted from 709 nm to 594 nm (Fig. 5, black line).

3.3 Composition effect on the energy band and optical properties of CIS and ZCIS QDs

Based on our results, reducing the Cu : In ratio in the CIS QDs and incorporating Zn to form alloyed ZCIS QDs are both feasible strategies for bandgap engineering. The evolution of

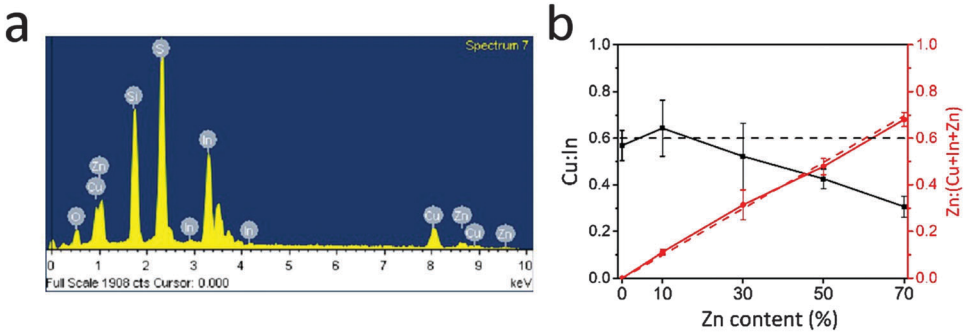

Fig. 4 EDX analysis of the synthesized ZCIS QDs. (a) A typical EDX spectrum of 30% ZCIS QDs. (b) EDX showing the Cu : In ratio and Zn proportion (solid line) in the synthesized ZCIS QDs as a function of their corresponding feed ratio (dashed line).

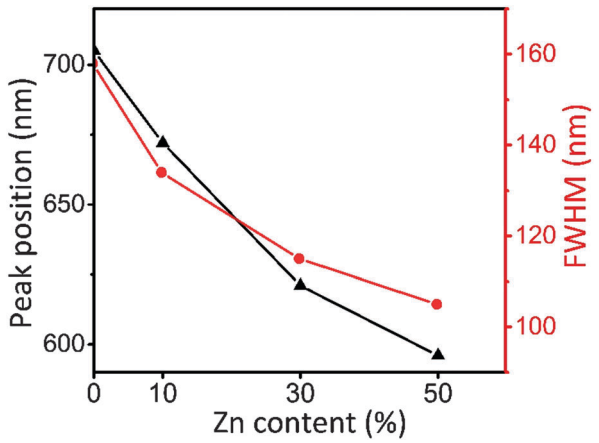

Fig. 5 Evolution of the PL peak position (triangle) and FWHM (circle) with increasing Zn content in ZCIS QDs.

optical bandgaps was illustrated by plotting $(ah\nu)^2$ *vs.* $h\nu$ derived from absorption spectra (the molar concentration of the samples is the same) and extrapolating the linear portion to intercept the x abscissa (Fig. 6).[59,60] The widening of the bandgap when reducing the Cu : In ratio or increasing the Zn content could be qualitatively confirmed from the continuous right shift of these derived curves. From curves with good linearity, the bandgaps of CIS QDs with a Cu : In ratio of 0.14 and 0.07 were estimated to be 2.73 eV and 2.78 eV (Fig. 6a, dash line) and those of the ZCIS QDs with a Zn content of 50% and 70% were calculated to be 2.75 eV and 2.94 eV (Fig. 6b, dashed line). Although a similar bandgap widening effect was observed, the influences of adjusting the Cu : In ratio or the Zn content on the QD optical properties were different. First, in comparison with tuning the Cu : In ratio, the incorporation of Zn resulted in a more pronounced blue shift in the absorption onset and in the UV region (Fig. 1b and 2b). In other words, the ZCIS QDs exhibit a larger absorption coefficient near the bandgap energy while the CIS QDs show a broader distribution of the absorption energy levels. This indicated the formation of a more homogeneous energy band in the ZCIS QDs. Second, varying the Zn content ratio resulted in a continuous blue-shift of the PL spectra, while similar results cannot be obtained by altering the Cu : In ratio in CIS QDs (Fig. 1c and 2c). This indicates that the gap between the donor and acceptor energy band of the ZCIS QDs was widened as the widening of the bandgap while the same trend was not observed for the CIS QDs. Based on the discussion above, the incorporation of Zn into CIS QDs might be an effective strategy to achieve a more homogeneous energy band, enhanced PL intensity, narrowed emission spectra and a wide range of emission wavelength tunability. The diameters of 0%, 30% and 70% ZCIS QDs determined from TEM results (Fig. 1a, 2a and Fig. S2, ESI†) are 4–7 nm and close to their Bohr exciton radius (5.0 nm for ZnS and 8.0 nm for $CuInS_2$), which further confirms that the composition control is the main cause for the tunable bandgap and optical properties.[21] Additionally, tuning the composition ratio is a more controllable strategy for adjusting the band gap and optical properties in these ZCIS QDs compared to the size control, because wavelength of their absorption/emission profiles was almost unchanged over the reaction time (Fig. S3, ESI†).

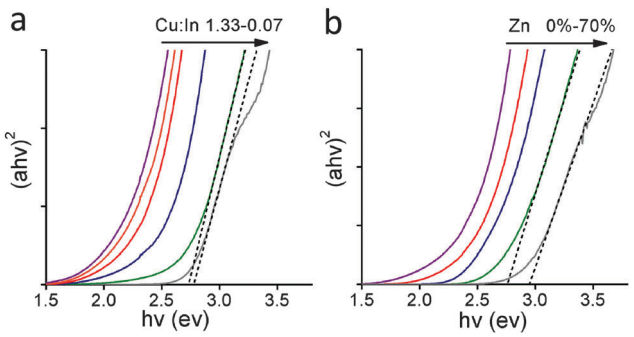

Fig. 6 Evolution of the optical bandgap of (a) CIS QDs with a reducing Cu : In ratio and (b) ZCIS QDs with increasing Zn content.

3.4 Effect of ZnS shell growth on the optical properties of CIS and ZCIS QDs

An additional ZnS shell was deposited on the ZCIS QD surface for improving their PL efficiency and enhancing their optical stability. Because of small lattice mismatch with $CuInS_2$,[32,40] ZnS is expected to have a similar lattice parameter with ZCIS. Also, the band alignment of ZCIS and ZnS[22] allows type-I structure formation for effective surface passivation. For 30% ZCIS QDs and their core/shell structures, the hydrodynamic

diameters were estimated to be 4.8 ± 0.9 nm and 6.7 ± 0.9 nm, respectively (Fig. 7a). The interplanar spacings measured from the FFT pattern of the HRTEM are 0.19 nm, 0.32 nm, 0.30 nm and 0.29 nm (Fig. S4, ESI†), in agreement with the zinc blende ZnS phase, the tetragonal CIS phase and their alloyed structure. As expected, the resulted ZCIS/ZnS QDs showed enhanced PL intensity. The QY of 30% ZCIS QDs was improved from 1.4% to 4.7% after ZnS coating (Fig. 7b). As an example, Fig. 8a shows the PL spectra of 30% ZCIS QDs before and after shell deposition. Compared to the ZCIS core QDs, the ZnS coated QDs exhibited enhanced emission intensity and a blue-shifted PL peak. However, this blue shift was much less pronounced as compared to that observed in CIS/ZnS QDs. As observed in Fig. 8b, the blue shifts for CIS QDs and 10%, 30% and 50% ZCIS QDs are 42 nm, 10 nm, 4 nm, 1 nm, respectively. The inhibition of the blue shift in ZCIS/ZnS could be attributed to the weakened lattice strain or the reduced cation exchange due to the existing Zn on the core surface.[56]

Time-resolved PL measurements were carried out to investigate the recombination process in ZCIS and ZCIS/ZnS QDs, the decay curves were fitted with double-exponential, and the fitting parameters are summarized in Fig. 9 and Table S2 (ESI†). The transient kinetics can be decomposed into a fast and slow decay component, of which the dynamics are on the time scales of several nanoseconds and more than 100 ns, respectively. The fast decay component is usually contributed to the non-radiative recombination and the slow decay component is consistent with the donor–acceptor recombination related to internal defects.[29,52,61] After coating with the ZnS shell, the average lifetime of the 30% ZCIS QDs was prolonged from 50 to 130 ns (Fig. 9). The significant reduction of the fast decay component after ZnS shell growth implies that the nonradiative recombination pathways can be effectively suppressed upon surface trap passivation. Additionally, growth of the ZnS shell may also lead to delocalization of the electron wave function into the shell region and reduce the electron/hole wave function overlap.[62] This change will lower the chance of the electron–hole recombination and prolong both the nonradiative and radiative processes, slightly. By comparing the decay curves of the CIS/ZnS QDs and ZCIS/ZnS QDs (Fig. S5, ESI†), no significant difference in the fluorescence lifetime can be detected, suggesting similar radiative channels of the two types of QDs.

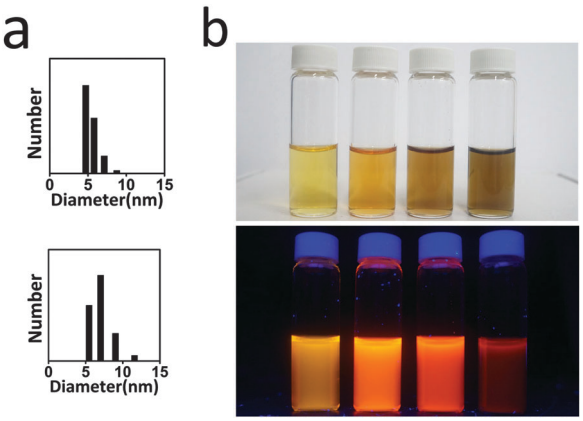

Fig. 7 Synthesis of ZCIS/ZnS QDs. (a) Hydrodynamic particle size distributions of 30% ZCIS QDs (top) and 30% ZCIS/ZnS QDs (bottom). (b) Water dispersion of ZCIS/ZnS QDs (left to right, 50%, 30%, 10%, 0% Zn content) under natural light (top) and UV light (bottom).

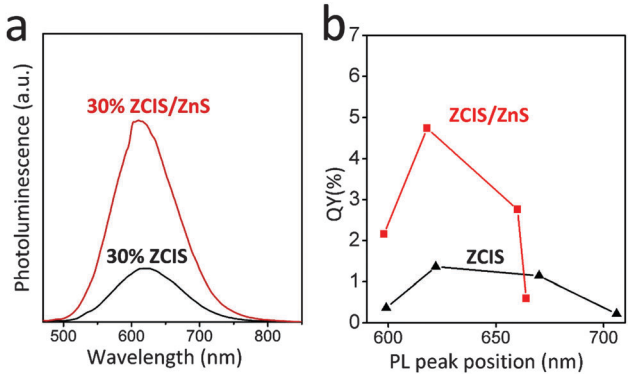

Fig. 8 (a) PL spectra of 30% ZCIS QDs before and after the ZnS shell growth. (b) PL QY and PL peak emission wavelength of ZCIS and ZCIS/ZnS QDs. The Zn content from left to right is 50%, 30%, 10% and 0%, respectively.

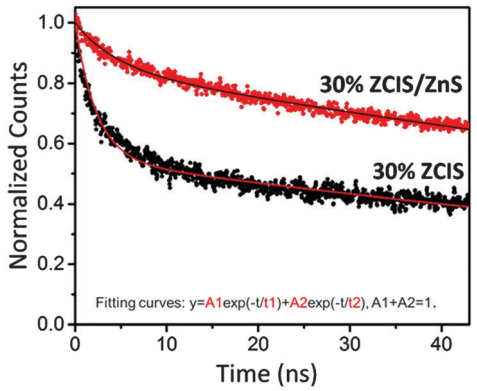

Samples	A1	t1 (ns)	A2	t2 (ns)	Average lifetime (ns)
30%ZCIS	0.44995	2.32656	0.55005	125.7231	49.92455
30%ZCIS/ZnS	0.14501	4.38184	0.85499	154.4516	130.2557

Fig. 9 Luminescence decay curves and fitted curves (solid line) of the 30% ZCIS QDs and 30% ZCIS/ZnS QDs. The fitting parameters are shown in the table.

3.5 Cell imaging and cell viability study of ZCIS/ZnS QDs

For *in vitro* imaging, photostability of the synthesized ZCIS/ZnS QDs was firstly examined under continuous UV irradiation (Fig. S6, ESI†). 30% ZCIS/ZnS QDs were used for optical imaging of RAW264.7 macrophages (Fig. 10). The cells stained with DAPI and QDs exhibited delocalized emissions from the cell nucleus and cytoplasm, which demonstrates the potential of using the aqueous synthesized ZCIS/ZnS QDs for cell imaging. To evaluate their cytotoxicity, MTT assay was performed on the 30% ZCIS/ZnS QDs. These ZCIS/ZnS QDs are almost nontoxic to macrophage cells (cell viability >90%) at a concentration of 200 μg mL^{-1} (Fig. 11). It should be noted that the concentration we used for the *in vitro* imaging in Fig. 10 is 20 μg mL^{-1}, which is nontoxic to RAW264.7 macrophages, according to our MTT results.

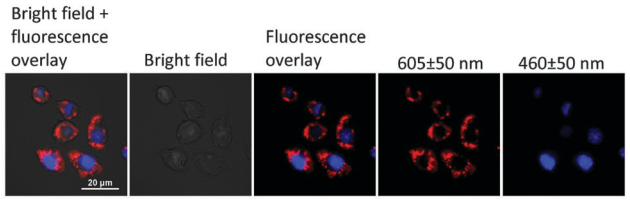

Fig. 10 Fluorescent imaging of RAW264.7 macrophage cells using 30% ZCIS/ZnS QDs. The cell nucleus was stained with DAPI.

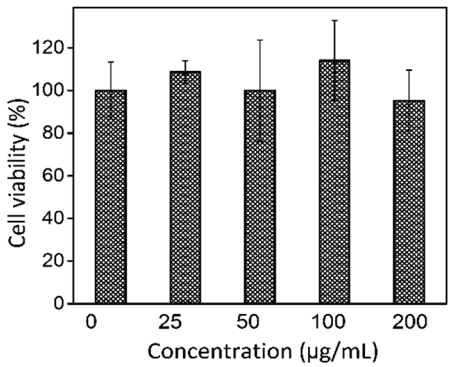

Fig. 11 Cell viability of RAW264.7 macrophages treated with 30% ZCIS/ZnS QDs for 24 h (n = 6).

4. Conclusions

In this work, the Zn–Cu–In–S (ZCIS) QDs were synthesized *via* a facile aqueous route at a low temperature (100 °C). Before preparing the ZCIS QDs, Cu–In–S (CIS) QDs were first synthesized and showed a multi-peak photoluminescence with the intensity dependent on the Cu : In ratio. Upon incorporating Zn into the CIS QDs, the PL intensity was significantly enhanced at the Zn content ratio of 10% and 30%, while further increasing the Zn content led to a decrease in the PL. Simultaneously, the FWHM was observed to narrow down, reflecting a more homogeneous irradiation in ZCIS QDs. The incorporation of Zn also resulted in a blue shift for the absorption and PL spectra, which indicated the widening of the QD bandgap. The influence of the Cu : In ratio and Zn content on their band gap and optical properties is compared and discussed. Overall, the incorporation of Zn into CIS QDs is an effective strategy to achieve a more homogeneous absorption band, enhance the PL intensity, narrow down the emission spectral width and increase the ability to tune the emission wavelength of the nanoparticles. Then, a ZnS shell was deposited on the ZCIS QDs and the resulting ZCIS/ZnS QDs showed enhanced PL intensity and prolonged fluorescence lifetime. Using the synthesized ZCIS/ZnS QDs, we examined the feasibility of employing them for imaging of macrophage cells. In macrophages cells, QDs and DAPI exhibited delocalized fluorescence signals from the cytoplasm and the cell nucleus indicating the nonspecific *in vitro* uptake of the QDs. The biocompatibility of these ZCIS/ZnS QDs further demonstrated their potential for future biophotonics applications.

Acknowledgements

This work was supported by the Singapore Ministry of Education (Grants Tier 2 MOE2010-T2-2-010 (M4020020.040 ARC2/11) and Tier 1 M4010360.040 RG29/10), NTU-NHG Innovation Collaboration Grant (No. M4061202.040), A*STAR Science and Engineering Research Council (No. M4070176.040) and School of Electrical and Electronic Engineering at NTU.

Notes and references

1 M. Bruchez, M. Moronne, P. Gin, S. Weiss and A. P. Alivisatos, *Science*, 1998, **281**, 2013–2016.
2 B. Dubertret, P. Skourides, D. J. Norris, V. Noireaux, A. H. Brivanlou and A. Libchaber, *Science*, 2002, **298**, 1759–1762.
3 J. M. Klostranec and W. C. Chan, *Adv. Mater.*, 2006, **18**, 1953–1964.
4 S. J. Rosenthal, J. C. Chang, O. Kovtun, J. R. McBride and I. D. Tomlinson, *Chem. Biol.*, 2011, **18**, 10–24.
5 Y. Wang, R. Hu, G. Lin, I. Roy and K.-T. Yong, *ACS Appl. Mater. Interfaces*, 2013, **5**, 2786–2799.
6 C. M. Tyrakowski and P. T. Snee, *Phys. Chem. Chem. Phys.*, 2014, **16**, 837–855.
7 S. J. Cho, D. Maysinger, M. Jain, B. Röder, S. Hackbarth and F. M. Winnik, *Langmuir*, 2007, **23**, 1974–1980.
8 J. L. Pelley, A. S. Daar and M. A. Saner, *Toxicol. Sci.*, 2009, kfp188.
9 H. S. Choi, W. Liu, P. Misra, E. Tanaka, J. P. Zimmer, B. I. Ipe, M. G. Bawendi and J. V. Frangioni, *Nat. Biotechnol.*, 2007, **25**, 1165–1170.
10 K.-T. Yong, H. Ding, I. Roy, W.-C. Law, E. J. Bergey, A. Maitra and P. N. Prasad, *ACS Nano*, 2009, **3**, 502–510.
11 T. Pons, E. Pic, N. Lequeux, E. Cassette, L. Bezdetnaya, F. Guillemin, F. Marchal and B. Dubertret, *ACS Nano*, 2010, **4**, 2531–2538.
12 Y. Du, B. Xu, T. Fu, M. Cai, F. Li, Y. Zhang and Q. Wang, *J. Am. Chem. Soc.*, 2010, **132**, 1470–1471.
13 F. Erogbogbo, K.-T. Yong, I. Roy, G. Xu, P. N. Prasad and M. T. Swihart, *ACS Nano*, 2008, **2**, 873–878.
14 N. Kenneth, *Nanoscale*, 2011, **3**, 2023–2027.
15 Y. Zhang, G. Hong, Y. Zhang, G. Chen, F. Li, H. Dai and Q. Wang, *ACS Nano*, 2012, **6**, 3695–3702.
16 J.-H. Liu, S.-T. Yang, X.-X. Chen and H. Wang, *Curr. Drug Metab.*, 2012, **13**, 1046–1056.
17 K. T. Yong, W. C. Law, I. Roy, Z. Jing, H. Huang, M. T. Swihart and P. N. Prasad, *J. Biophotonics*, 2011, **4**, 9–20.
18 K. Littau, P. Szajowski, A. Muller, A. Kortan and L. Brus, *J. Phys. Chem.*, 1993, **97**, 1224–1230.
19 R. Xie, D. Battaglia and X. Peng, *J. Am. Chem. Soc.*, 2007, **129**, 15432–15433.
20 S. Chen, X. Gong, A. Walsh and S.-H. Wei, *Phys. Rev. B: Condens. Matter Mater. Phys.*, 2009, **79**, 165211.
21 D. Pan, D. Weng, X. Wang, Q. Xiao, W. Chen, C. Xu, Z. Yang and Y. Lu, *Chem. Commun.*, 2009, 4221–4223.
22 M. Xu, J. Zai, Y. Yuan and X. Qian, *J. Mater. Chem.*, 2012, **22**, 23929–23934.

23 B. Chen, H. Zhong, W. Zhang, Z. a. Tan, Y. Li, C. Yu, T. Zhai, Y. Bando, S. Yang and B. Zou, *Adv. Funct. Mater.*, 2012, **22**, 2081–2088.
24 N. Khemiri and M. Kanzari, *Thin Solid Films*, 2011, **519**, 7201–7206.
25 S. Li, Y. Chen, L. Huang and D. Pan, *Nanotechnology*, 2013, **24**, 395705.
26 S. Chen, X. Gong, A. Walsh and S.-H. Wei, *Appl. Phys. Lett.*, 2010, **96**, 021902.
27 S. Chen, J.-H. Yang, X. Gong, A. Walsh and S.-H. Wei, *Phys. Rev. B: Condens. Matter Mater. Phys.*, 2010, **81**, 245204.
28 L. Li, T. J. Daou, I. Texier, T. T. Kim Chi, N. Q. Liem and P. Reiss, *Chem. Mater.*, 2009, **21**, 2422–2429.
29 L. De Trizio, M. Prato, A. Genovese, A. Casu, M. Povia, R. Simonutti, M. J. Alcocer, C. D'Andrea, F. Tassone and L. Manna, *Chem. Mater.*, 2012, **24**, 2400–2406.
30 M. Michalska, A. Aboulaich, G. Medjahdi, R. Mahiou, S. Jurga and R. Schneider, *J. Alloys Compd.*, 2015, **645**, 184–192.
31 S. Liu, H. Zhang, Y. Qiao and X. Su, *RSC Adv.*, 2012, **2**, 819–825.
32 Y. Chen, S. Li, L. Huang and D. Pan, *Inorg. Chem.*, 2013, **52**, 7819–7821.
33 W.-W. Xiong, G.-H. Yang, X.-C. Wu and J.-J. Zhu, *ACS Appl. Mater. Interfaces*, 2013, **5**, 8210–8216.
34 D. Deng, Y. Chen, J. Cao, J. Tian, Z. Qian, S. Achilefu and Y. Gu, *Chem. Mater.*, 2012, **24**, 3029–3037.
35 M. G. Panthani, T. A. Khan, D. K. Reid, D. J. Hellebusch, M. R. Rasch, J. A. Maynard and B. A. Korgel, *Nano Lett.*, 2013, **13**, 4294–4298.
36 C.-W. Chen, D.-Y. Wu, Y.-C. Chan, C. C. Lin, P.-H. Chung, M. Hsiao and R.-S. Liu, *J. Phys. Chem. C*, 2015, **119**, 2852–2860.
37 S. Hu, S. Zeng, B. Zhang, C. Yang, P. Song, T. J. H. Danny, G. Lin, Y. Wang, T. Anderson and P. Coquet, *Analyst*, 2014, **139**, 4681–4690.
38 R. M. Hodlur and M. K. Rabinal, *Chem. Eng. J.*, 2014, **244**, 82–88.
39 J. Cheng, D. Li, T. Cheng, B. Ren, G. Wang and J. Li, *J. Alloys Compd.*, 2014, **589**, 539–544.
40 W. Zhang and X. Zhong, *Inorg. Chem.*, 2011, **50**, 4065–4072.
41 J. Zhang, R. Xie and W. Yang, *Chem. Mater.*, 2011, **23**, 3357–3361.
42 T. Jiang, J. Song, H. Wang, X. Ye, H. Wang, W. Zhang, M. Yang, R. Xia, L. Zhu and X. Xu, *J. Mater. Chem. B*, 2015, **3**, 2402–2410.
43 L. De Trizio, M. Prato, A. Genovese, A. Casu, M. Povia, R. Simonutti, M. J. P. Alcocer, C. D'Andrea, F. Tassone and L. Manna, *Chem. Mater.*, 2012, **24**, 2400–2406.
44 M. Uehara, K. Watanabe, Y. Tajiri, H. Nakamura and H. Maeda, *J. Chem. Phys.*, 2008, **129**, 134709.
45 D.-E. Nam, W.-S. Song and H. Yang, *J. Mater. Chem.*, 2011, **21**, 18220–18226.
46 R. Jayakrishnan, T. T. John, C. S. Kartha, K. Vijayakumar, T. Abe and Y. Kashiwaba, *Semicond. Sci. Technol.*, 2005, **20**, 1162.
47 N. Poornima, T. Vimalkumar, V. Rajeshmon, C. S. Kartha and K. Vijayakumar, *Int. J. Photoenergy*, 2013, **2013**, 105796.
48 X. Cao, L. Gu, L. Zhuge, W. Qian, C. Zhao, X. Lan, W. Sheng and D. Yao, *Colloids Surf., A*, 2007, **297**, 183–190.
49 J. Park and S.-W. Kim, *J. Mater. Chem.*, 2011, **21**, 3745–3750.
50 Z. Leng, L. Huang, F. Shao, Z. Lv, T. Li, X. Gu and H. Han, *Mater. Lett.*, 2014, **119**, 100–103.
51 F. W. Wise, *Acc. Chem. Res.*, 2000, **33**, 773–780.
52 Y.-K. Kim, S.-H. Ahn, K. Chung, Y.-S. Cho and C.-J. Choi, *J. Mater. Chem.*, 2012, **22**, 1516–1520.
53 A. M. Smith, A. M. Mohs and S. Nie, *Nat. Nanotechnol.*, 2009, **4**, 56–63.
54 I. T. Kraatz, M. Booth, B. J. Whitaker, M. G. Nix and K. Critchley, *J. Phys. Chem. C*, 2014, **118**, 24102–24109.
55 W. Guo, N. Chen, C. Dong, Y. Tu, J. Chang and B. Zhang, *RSC Adv.*, 2013, **3**, 9470–9475.
56 W. Guo, *Theranostics*, 2013, **3**, 99.
57 H. Nakamura, W. Kato, M. Uehara, K. Nose, T. Omata, S. Otsuka-Yao-Matsuo, M. Miyazaki and H. Maeda, *Chem. Mater.*, 2006, **18**, 3330–3335.
58 H. Ueng and H. Hwang, *J. Phys. Chem. Solids*, 1989, **50**, 1297–1305.
59 C. Yang, B. Zhou, S. Miao, C. Yang, B. Cai, W.-H. Zhang and X. Xu, *J. Am. Chem. Soc.*, 2013, **135**, 5958–5961.
60 B. Mao, C.-H. Chuang, J. Wang and C. Burda, *J. Phys. Chem. C*, 2011, **115**, 8945–8954.
61 W.-D. Xiang, H.-L. Yang, X.-J. Liang, J.-S. Zhong, J. Wang, L. Luo and C.-P. Xie, *J. Mater. Chem. C*, 2013, **1**, 2014–2020.
62 Y.-K. Kim, Y.-S. Cho, K. Chung and C.-J. Choi, *Proc. SPIE*, 2011, 8094.